

In-situ fruit analysis by means of LiDAR 3D point cloud of normalized difference vegetation index (NDVI)

Nikos Tsoulas, Kowshik Kumar Saha, Manuela Zude-Sasse*

Leibniz Institute for Agricultural Engineering and Bioeconomy (ATB), Max-Eyth-Allee 100, 14469 Potsdam, Germany

ARTICLE INFO

Keywords:

Chlorophyll
Digitization
LiDAR
Orchard
Sensor
Tree

ABSTRACT

A feasible method to analyse fruit at the tree is requested in precise production management. The employment of light detection and ranging (LiDAR) was approached aimed at measuring the number of fruit, quality-related size, and ripeness-related chlorophyll of fruit skin.

During fruit development (65 – 130 day after full bloom, DAFB), apples were harvested and analysed in the laboratory ($n = 225$) with two LiDAR laser scanners measuring at 660 and 905 nm. From these two 3D point clouds, the normalized difference vegetation index ($NDVI_{LiDAR}$) was calculated. The correlation analysis of $NDVI_{LiDAR}$ and chemically analysed fruit chlorophyll content showed $R^2 = 0.81$ and $RMSE = 3.63\%$ on the last measuring date, when fruit size reached 76 mm.

The method was tested on 3D point clouds of 12 fruit trees measured directly in the orchard, during fruit growth on five measuring dates, and validated with manual fruit analysis in the orchard ($n = 4632$). Point clouds of individual apples were segmented from 3D point clouds of trees and fruit $NDVI_{LiDAR}$ were calculated. The non-invasively obtained field data showed good calibration performance capturing number of fruit, fruit size, fruit $NDVI_{LiDAR}$, and chemically analysed chlorophyll content of $R^2 = 0.99$, $R^2 = 0.98$ with $RMSE = 3.02\%$, $R^2 = 0.65$ with $RMSE = 0.65\%$, $R^2 = 0.78$ with $RMSE = 1.31\%$, respectively, considering the related reference data at last measuring date 130 DAFB.

The new approach of non-invasive laser scanning provided physiologically and agronomically valuable time series data on differences in fruit chlorophyll affected by the leaf area to number of fruit and leaf area to fruit fresh mass ratios. Concluding, the method provides a tool for gaining production-relevant plant data for, e.g., crop load management and selective harvesting by harvest robots.

1. Introduction

Consumption of fresh fruit is recommended and worldwide an estimate of 883 million t, with a share of 10 % for apple, were produced in 2020 (FAO, 2022). Consumption of apples (*Malus × domestica* Borkh.) is globally high regardless of local production capability resulting in apple being one of the most traded fruit in the world. During ontogenesis of apple, the harvest maturity is determined by the complex ripening process of fruit, which affects fruit storability and market quality (Jones et al., 1965; Cusmano et al., 2018). Apple is a climacteric fruit, showing enhanced ethylene production and respiration rate at commercial harvest (Nelson, 1940; Biale, 1964; Hewitt and Dhingra, 2020). Apples harvested too early may cause reduced blush colour, lack of cultivar-specific aroma, and harsh cortex tissue, whereas too late harvest reduces storability resulting in postharvest loss and food waste along the

supply chain. Visual monitoring of apple peel colour is widely performed subjectively to identify the harvest-ripe fruit during manual harvest. During climacteric, chlorophyll content decreases and, therefore, change of chlorophyll during fruit development can be employed as an indicator for the ripening progress (Knee, 1980; Zude-Sasse et al., 2002; Han et al., 2018). To gain resilient fruit production, instrumental monitoring of fruit size and ripeness information is requested in production measures such as crop load management, yield estimation, and determining the harvest date (Solovchenko et al., 2005; Zude-Sasse et al., 2016; Delong et al., 2020). Furthermore, the development of harvest robots is needed to enable cost effective harvesting. For guiding the robot to the ripe fruit, fruit size and chlorophyll information are important variables.

At the present state of knowledge, instrumental non-destructive analysis of fruit chlorophyll is established based on color analysis such

* Corresponding author.

E-mail address: mzude@atb-potsdam.de (M. Zude-Sasse).

as employed for analysis of fruit in production and postharvest in sorting lines (Walsh et al., 2020). Here, the chlorophyll content is represented in the red channel of red, green, blue (RGB) cameras or, e.g., along the a^* axis of $L^*a^*b^*$ color space. Spectrophotometry has been employed for more specific fruit pigment analysis (Knee, 1980; Merzlyak et al., 1999; Zude-Sasse et al., 2002) and became commercially available as handheld systems (Walsh et al., 2020) and for inline grading to obtain information on the fruit ripeness stage. Furthermore, spectral-optical analysis with enhanced wavelength resolution enabled the measurement of individual chlorophylls at Q band of absorption of chlorophyll pool, such as chlorophyll_A, _B, and pheophytin_A (Seifert and Zude-Sasse, 2016). Such non-destructive methods can be applied in laboratory or packhouse conditions, however, results are affected by varying lighting conditions appearing in field applications.

In outdoor measurements, the normalized difference vegetation index (NDVI) was introduced using the sun as light source and measuring the reflectance (Rouse et al., 1973). The NDVI examines the difference/sum ratio of reflectance at a shortwave near infrared (SWNIR) radiation band in the range between 700 nm and 1100 nm and at a red wavelength range, frequently measured at 660 nm (SWNIR-RED)/(SWNIR + RED). The index was initially used to assess the presence of vegetation and its application was confirmed in many studies (Zhou et al., 2001; Anyamba and Tucker, 2005; Tucker et al., 2005). Meanwhile, the NDVI and other vegetation indices were applied in remote sensing approaches of agricultural production for estimating, e.g., vegetation cover, leaf area index (Bannari et al., 2009), and chlorophyll content of tree canopy (Li et al., 2018). Alternatively, multispectral cameras were mounted on unmanned aerial platforms to relate the canopy NDVI with vigor of fruit trees (Ballester et al., 2018; Ampatzidis et al., 2019), yield and fruit quality prediction (Kasimati et al., 2022).

Considering NDVI in fruit analysis, measurements were performed in close contact of fruit and sensor, capturing a light source and receiver. The fruit NDVI was introduced and compared to other data processing methods for predicting the fruit chlorophyll content (Zude, 2003). Again, various indices were tested (Zude-Sasse et al., 2002; Ziosi et al., 2008), and NDVI was confirmed to be sensitive in the relevant range of fruit chlorophyll content. In apple, the NDVI measured in remittance geometry was reported as robust for predicting the fruit chlorophyll in comparison to fluorescence readings (Kuckenberger et al., 2008). In stone fruit, the use of time-resolved spectral-optical analysis enabled to separate the absorption and scattering effects of the fruit tissue, enhancing the accuracy of NDVI analysis (Seifert et al., 2015). However, all methods are requested to be carried out in close proximity to the fruit and varying light conditions alter the signal (Dassot et al., 2011). The feasible usage of the chlorophyll data on a robot requires the classification of various chlorophyll classes on the tree capturing the distance between the robot and the fruit in the canopy, which may be assumed as 0.3 – 1.6 m.

Three-dimensional (3D) vision systems, such as light detection and ranging (LiDAR) laser scanning may overcome the limitations of established spectral-optical point or 2D imaging methods (Gongal et al., 2018; Walsh et al., 2020; Keller et al., 2022). LiDAR has been used in remote sensing application in arable farming and forestry due to its capability to provide 3D geometric information of vegetation in field conditions (Peña et al., 2017; Deery et al., 2021). Furthermore, estimation methods for structural parameters and chlorophyll content in broadleaf plants were developed employing terrestrial LiDAR sensor (Eitel et al., 2010). In almond orchard, the mapping of flowers and fruit was achieved (Underwood et al., 2016). Advancement of terrestrial LiDAR sensors facilitates to acquire also the intensity of backscattered reflection at each point measured. Thus, besides geometric information, intensity of reflected signal becomes available as shown earlier for the segmentation of apple fruit (Gené-Mola et al., 2019; Tsoulas et al., 2020). Subsequently, simulation studies were published to quantify chlorophyll content of broadleaf forest trees, using terrestrial LiDAR to estimate the leaf area and hyperspectral satellite images to extract the

chlorophyll content (Cifuentes et al., 2018). Showing that variability in both chlorophyll content and leaf area can be deduced from the variation in the NIR part of the spectrum. Several studies proved the application of LiDAR 3D point cloud with intensity or full waveform information for detecting the overall chlorophyll status of vegetation (Watt and Donoghue, 2005; Clawges et al., 2007). Wei et al., (2012), developed a multi wavelength LiDAR to relate the foliage nitrogen uptake with seven vegetation indices, including NDVI and presenting an $R^2 = 0.82$. Despite the agronomical importance of fruit chlorophyll and the known relationship of fruit chlorophyll content with the NDVI, the fruit NDVI and its development during the growth season were not reported based on LiDAR data so far.

Therefore, objectives of the present study were to (i) develop a method for estimating the segmented NDVI of fruit obtained with LiDAR at 660 and 905 nm ($NDVI_{LiDAR}$), (ii) verify the relationship of temporally measured $NDVI_{LiDAR}$ with the fruit chlorophyll content (iii) characterizing the change of fruit $NDVI_{LiDAR}$ with leaf area to fruit ratio and leaf area to fresh mass ratio.

2. Materials and methods

2.1. Site description

The experiment was conducted in the experimental apple orchard located in Potsdam-Marquardt, Germany (Latitude: 52.466274° N, Longitude: 12.57291° E) of Leibniz Institute for Agricultural Engineering and Bioeconomy (ATB). The field is located on an 8 % slope with southeast orientation, planted with trees of *Malus × domestica* Borkh. ‘Gala-Brookfield’, ‘JonaPrince’, and pollinator trees ‘Red Idared’ each on M9 rootstock with 0.95 m distance between trees, trained as slender spindle with an average tree height of 2.8 m. Trees were statically supported by horizontally parallel wires.

All measurements were conducted five times during fruit development. Trees were scanned 65 days after full bloom (DAFB₆₅) during the end of cell division stage of fruit, before the Brookfield-typical red blush colour (Sadar et al., 2013) appeared, subsequently during fruit development 75, 90, 105, and 130 days after full bloom (DAFB₇₅, DAFB₉₀, DAFB₁₀₅, DAFB₁₃₀, respectively). Twelve trees of Gala-Brookfield were analysed by means of the non-invasive sensor system and fruit were sampled from these trees for the lab measurements. Further neighboring trees were used for destructive measurements such as leaf area analysis after defoliation.

3. LiDAR measurements in field and laboratory conditions

3.1. Field data acquisition

A phenotype sensing system was mounted on a circular conveyor platform, established in the experimental apple orchard (TechGarden, ATB), employing an electrical engine working with 50 Hz (DRN71, SEW Eurodrive, Germany) and stainless-steel chain with mechanical suspensions for varying plant sensors (Fig. 1). Two mobile 2D LiDAR sensors emitting at wavelength 905 nm (LMS-511, Sick AG, Waldkirch, Germany) and 660 nm (R2000, Pepperl Fuchs, Mannheim, Germany) were mounted horizontally on the metal frame at 0.7 m above the ground level (Fig. 1). The LMS-511 and R2000 were configured with 0.1667° and 0.029° angular resolution, 25 and 20 Hz scanning frequency, scanning angle of 180° and 270°, 1081 and 12,600 points per scan, 20 and 232 hits per cm², 20 and 10 W consumption power, respectively. The field scanning was carried out during the day with an average global radiation of 220 W m⁻². A real time kinematic global navigation satellite system (RTK-GNSS; AgGPS 542, Trimble, Sunnyvale, CA, USA) was used to geo-reference the data and an inertial measurement unit (IMU; MTi-G-710, XSENS, Enschede, Netherlands) was applied to acquire orientation information, with both sensors placed on the sensor frame. The IMU was placed 0.3 m aside from the LiDAR



Fig. 1. Sensors mounted on a. chain conveyor to measure entire trees in the experimental orchard, and b. tooth-belt conveyor to measure individual fruit in dark room conditions.

sensor, while the receiver antenna of RTK-GNSS was mounted 0.6 m above the laser scanner. The platform enables the automated monitoring of 109 trees from both sides around one row of 84 m length, of which 12 trees were analysed in this study considering field and lab data. The circular conveyor moved at 10 mm s^{-1} ($\pm 0.02 \text{ mm}$ accuracy) forward speed.

3.2. Laboratory LiDAR data acquisition

After each measurement with the phenotyping sensor system, apple samples ($n = 45$) were collected for reference analyses. A subsample of apples ($n = 10$), from the 45 apple-batch, was additionally scanned in the laboratory on the five measuring dates. The measurement was carried out in a dark room, controlled ventilation and temperature. A rigid linear toothbelt conveyor system (Module 115/42, IEF Werner, Germany) of 2 m length, equipped with servo positioning controller (LV-servoTEC S2, IEF Werner, Germany), was mounted on a rigid aluminium frame to carry the two LiDAR sensors and scan each apple individually (Fig. 1). The linear conveyor moved at 20 mm s^{-1} ($\pm 0.05 \text{ mm}$ accuracy) forward speed.

4. LiDAR data processing

4.1. Point cloud reconstruction

The 3D point cloud dataset was generated and processed in the Computer Vision Toolbox™ of MATLAB (2018b, Mathworks, Natick, MA, USA). Board targets, coated with white barium sulphate (BaSO₄, CAS Number: 7727-43-7, Merck, Germany) for maximum values and blackened urethane (S black, Avian Technologies, New London, NH, USA) for minimum values were used to calibrate the apparent reflectance intensity (R_{ToF}) of the LiDARs, obtaining the R_{ToF} [%] at 905 and 660 nm for each point in the 3D point cloud.

Rigid translations and rotations were applied on each point of 3D cloud, while alignment of pairing tree sides was carried out with iterative closest point algorithm (Tsoulias et al., 2019). Trees were segmented based on stem position and planting distance to gain points per tree (PPT) from each plant (Tsoulias et al., 2019). More specifically, the bivariate point density histogram enabled the detection of the peak of laser hits for each individual tree based in the assumption that the stem points appear in the center of the canopy. According to the tree training system as slender spindle, the area closer to the stem position

can be assumed to appear with enhanced frequency. The coordinates of the estimated stem position were utilized as the center for the segmentation cylinders in order to obtain the points that belonged to each individual tree. The points within the boundaries of the cylinder were segmented and considered as the tree points. In the laboratory, data were recorded and all measured distances were filtered to remove surrounding points. As the apple samples were scanned from 0.9 m distance, the distance filter was configured between 0.75 and 1.25 m. Distant filtering also helped to reduce the raw data file size and resulted in less processing time in further steps. Using the corresponding distances in x and y direction of vertical line of scan. The linear movement of the LiDAR scanner was in z direction and displacement in this direction was calculated by forward speed and time difference between each vertical line of scan.

For all data sets from field and laboratory, the 3D point clouds at 660 nm and 905 nm were further processed capturing data sets of position in local Cartesian x,y, z coordinate system and reflected intensity of each point (R_{ToF}).

4.2. Leaf area estimation

For each point of 3D tree cloud the geometric feature of linearity (L) and curvature (C) were calculated applying the k-nearest neighbours (KNN) algorithm in the local neighbourhood of points $P_i = [x_i \ y_i \ z_i]$ (Tsoulias et al., 2022). The total number of P_i within each tree's cloud was used to estimate the mean of all nearest neighbors. The latter was used to produce eigenvalues ($\lambda_1, \lambda_2, \lambda_3$), after decomposition of covariance matrix. The probability density function was performed to define the thresholds of L , C , LiDAR's backscattered intensity (R_{ToF}) to distinguish the 3D points of woody parts (W) from leaves. The value with the highest likelihood (mode) within L_W , C_W , $R_{ToF,W}$ distribution was used as threshold ($R_{th,W}$; $C_{th,W}$; and $L_{th,W}$). Points that fulfilled the criteria of $L_W \leq L_{th,W}$, $C_{th,W} \leq C_W$, and $R_{th,W} \leq R_{ToF,W}$ were segmented and categorized as wood.

Segmented points of wood were subtracted from the total number of PPT. A linear regression model was built to express the relationship between manually obtained leaf area data and remaining PPT, separately for each growth stage. The model performance was evaluated based on the adjusted coefficient of determination in calibration (R_{adj}^2) and and root mean square error (RMSE). The linear calibration was applied to convert PPT into LA_{LiDAR} of each tree (Tsoulias et al., 2022).

4.3. Apple detection, counting, and sizing

For defining the position and shape of apples, the geometric feature of curvature (C) and R_{ToF} were used considering each point of the 3D tree point cloud (Tsoulias et al., 2020). Following the previous method, the local neighbors were decomposed and eigenvalues were produced. The values closer to 100, the higher the likelihood for shape of point appearance to be curved. Threshold values of apple points in terms of C and reflected intensity (C_A and $R_{ToF,A}$) were defined according to Tsoulias et al., (2020) by performing probability density function. The points that fulfilled the criteria of $C_{th,A} \leq C_A$, and $R_{th,A} \leq R_{ToF,A}$ were segmented and categorised as apple. Subsequently, a density-based scan algorithm (DBSCAN) was applied to find the point sets, using the mean manually measured diameter of fruit that was found in the neighborhood search radius and the value 10 as a minimum number of neighbors. The value of 10 was applied resulting from manually run tests showing that less neighboring points result in random appearance of sets. The maximum distance in x and y axes of fruit points was considered as diameter of each point set recognized as an apple (D_{LiDAR}). Thereafter, k -means clustering was applied to find the fruit center(s) in each apple cluster and count the number of fruit per tree ($Fruit_{LiDAR}$).

Subsequently, the ratio of leaf area to number of fruit per tree ($LA_{LiDAR}:Fruit_{LiDAR}$) was estimated in each growth stage in low and high sections of tree canopy determined by the wire structure at 1.8 m statically supporting the tree.

4.4. NDVI estimation

The point clouds of segmented apples was obtained from the two LiDAR laser scanners, which varied considering the point density due to different scanning frequency and angle resolution. The corresponding point clouds of the same apple were merged by means of a density histogram applied on segmented apple clouds (Fig. 2).

The x and y values of each point paired in bins of size 3.3 mm^2 , allowing to describe the underlying point density distribution of apple R_{ToF} as means of each bin within the grid of 40×40 bins within the shape of each fruit. The number of points in each bin varied according to the shape and size of apple. The bin's mean values allowed to use the corresponding values of both LiDAR systems for calculating the fruit normalised differential vegetation index ($NDVI_{LiDAR}$).

$$NDVI_{LiDAR} = \frac{R_{ToF,905} - R_{ToF,660}}{R_{ToF,905} + R_{ToF,660}}$$

Where $R_{ToF,905}$ and $R_{ToF,660}$ represent the reflected intensity measured at 905 and 660 nm, respectively. The derived $NDVI_{LiDAR}$ cloud of each apple was corrected for outliers by means of Gaussian filter with standard deviation of distribution equal to 1. The interquartile range, estimated by subtracting the points of lowest and highest quartile, were used in further calculations. The process was applied in all segmented fruit point clouds over the growth period (Fig. 2). The mean $NDVI_{LiDAR}$ of each fruit was processed further. The results were categorised in low (0–1.8 m) and high (1.8–2.6 m) sections of tree heights determined by

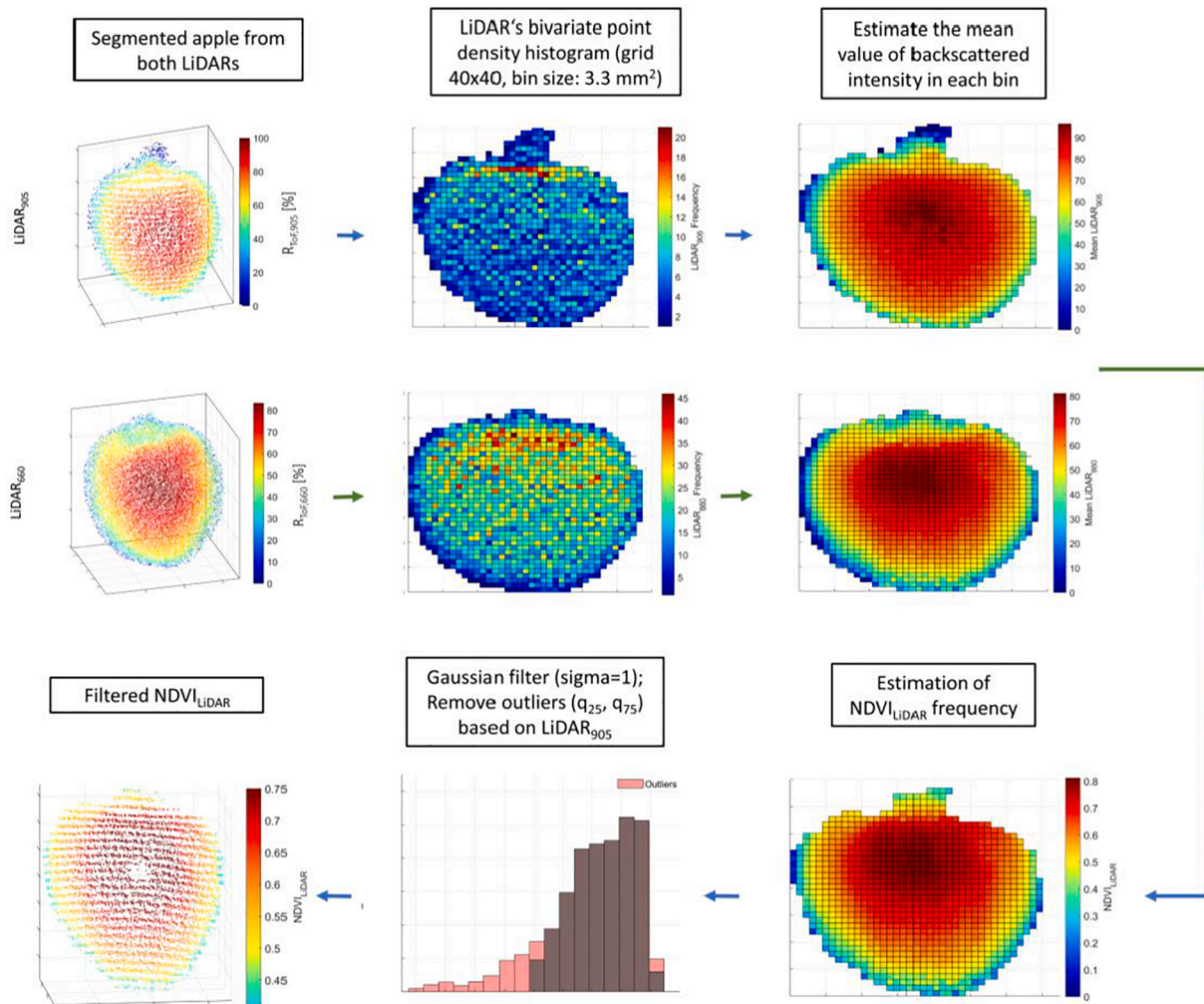


Fig. 2. Flow chart to calculate fruit $NDVI_{LiDAR}$ from segmented 3D fruit point clouds.

the wire structure.

5. Reference measurements

5.1. Leaf area

On each measuring date, 3 apple trees neighboring the monitored 12 trees were manually defoliated. The overall 15 trees were scanned before and after defoliation. The obtained leaf area per tree (LA_{Ref}) was manually recorded with a desktop scanner (Scanjet 4850, HP, USA) by counting the number of green pixels per leaf with a MATLAB script (Vers. 2018b, Mathworks, Natick, MA, USA). The area of 6241 pixel corresponded to 1 cm². The results were categorised in the low and high section of canopy determined by the wire structure.

5.2. Crop load and fruit quality

Fruit number ($Fruit_{Ref}$) was manually counted per tree ($n = 12$) in low and high sections of the canopy, separated by the construction wires at 1.8 m, on the last three measuring dates. Measurements of fruit diameter ($n = 180$) were recorded at the two tree height ranges over the growth period.

At each of the five measuring dates, 45 fruit were analysed in the laboratory. Fruit diameter [mm] was manually measured (D_{Ref}) in the laboratory by means of a digital calliper gauge considering the mean diameter of two measurements taken equatorially with 90° difference. The fruit fresh mass (FM) [kg] was measured by weighing each fruit sample.

The reference NDVI ($NDVI_{Ref}$) was recorded with a handheld spectrophotometer (Pigment Analyzer, PA1101, CP, Golm, Germany) in remittance geometry by placing the sensor probe on the fruit surface avoiding stray light with the silicon probe of the device. Also, these analyses were separated in low and high sections of tree canopy.

The chlorophyll content of skin and associated hypodermis tissue (2 mm thickness) of apples ($n = 45$) was destructively analysed at each measuring date over the fruit development. The chlorophyll_A, _B, and pheophytin_A contents were analysed by spectrophotometry after acetone/diethyl ether extraction by means of iterative multiple linear regression considering the standard spectra of the three chlorophylls (Pflanz and Zude, 2008).

Table 1

Reference data and LiDAR derived estimations with error analysis (mean bias error, MBE ; root mean squared error, $RMSE$; coefficient of determination, R^2) considering fruit number ($Fruit_{LiDAR}$), fruit diameter (D_{LiDAR}), and leaf area (LA_{LiDAR}) measured at the tree in five growth stages of apples in day after full bloom (DAFB). Results of leaf area corresponds to manually deafoiliated trees ($n = 3$).

		DAFB ₆₅	DAFB ₇₅	DAFB ₉₀	DAFB ₁₀₅	DAFB ₁₃₀
No. $Fruit_{Ref}$	Sum ($n = 12$ trees)	X	X	795	771	771
	Mean			65	64	65
	Max			84	84	84
	Min			19	19	19
No. $Fruit_{LiDAR}$	Sum	745	773	788	767	771
	Mean	66	71	71	70	70
	MBE	-4	-2	-1	1	0
	RMSE (%)	0.33	0.26	0.69	0.96	0.01
	R ²	0.88	0.96	0.96	0.99	0.99
D_{Ref} (mm)	Mean	35.5	48.3	59.1	61.4	76.1
	Max	41.7	52.5	65.0	66.0	83.0
	Min	32.0	41.4	52.0	56.0	68.0
D_{LiDAR} (mm)	Mean	35.8	48.4	59.1	61.5	76.1
	MBE	0.37	0.46	0.11	0.05	-0.08
	RMSE (%)	6.13	6.04	6.22	3.08	3.02
	R ²	0.85	0.87	0.86	0.95	0.98
LA_{Ref} (m ²)	Mean	6.40	6.41	6.47	6.48	6.54
	Max	6.48	6.51	6.54	6.55	6.56
	Min	6.26	6.26	6.20	6.41	6.47
LA_{LiDAR} (m ²)	Mean	6.41	6.51	6.54	6.50	6.60
	MBE	0.17	0.22	0.23	0.23	0.25
	RMSE (%)	3.14	3.03	3.12	2.42	6.36
	R ²	0.89	0.95	0.96	0.95	0.86

5.3. Data evaluation

Descriptive statistics were applied to all datasets capturing minimum, maximum, mean, standard deviation. A regression analysis was performed to quantify linear and logarithmic relationships between the manual measurements and LiDAR-derived data over the growing stages, and root mean square error ($RMSE$), mean bias error (MBE), coefficient of determination (R^2) were calculated. Descriptive statistics were carried out by Matlab (v.R2018b, Mathworks Inc., Natick, MA, USA).

6. Results and discussion

6.1. Fruit segmentation

Slender spindle form the major training system of apple trees in world-wide production, providing a 3D structure in which the fruit are more or less evenly distributed according to the success of the thinning measure. Yield monitoring is considered as an important step when implementing precision horticulture techniques in orchards. In the present study, fruit detection technique was applied to extract the number of fruit from the point cloud of LiDAR₉₀₅ and LiDAR₆₆₀ (Fig. S1). The fruit segmentation routine was described earlier (Tsoulas et al., 2020). The 3D point cloud data are provided as supplement.

The LiDAR₉₀₅ was used as a pilot sensor to segment the fruit, pointing to $R^2 = 0.99$ for the fruit detection (Table 1). The F1 values were 85.7, 87.3, 88.6, 91.3, 91.4 at DAFB₆₅, DAFB₇₅, DAFB₉₀, DAFB₁₀₅, DAFB₁₃₀, respectively. The highest difference between manually counted and estimated number of fruit was observed at DAFB₆₅, when mean apple size was $D_{Ref} = 35.5$ mm, reaching $R^2 = 0.88$. On the last measuring date, when the fruit reached their maximum size of $D_{Ref} = 76.1$ mm, $R^2 = 0.99$ was found. Differences appeared for individual trees, but the overall precision to count fruit was high (Table 1).

After fruit localization and fruit counting, the estimated fruit size (D_{LiDAR}) was compared to the manually measured diameter during the growth period (Table 1). The F1 values were 86.5, The D_{LiDAR} was related to the manual measurements, especially in the later stages, DAFB₁₀₅ and DAFB₁₃₀, resulting in $R^2 = 0.95$ and $R^2 = 0.98$ with $RMSE = 3.1\%$ and 3.0% , respectively. Generally, enhanced measuring uncertainty was noticed on the first two measuring dates, when fruit size was smaller. More specifically, a less pronounced relation was observed

on the first measuring date, presenting a slight overestimation of fruit size (Table 1). Similar good results were reported earlier on fruit detection and sizing at harvest (Gongal et al., 2018; Gene-Mola et al., 2019), whereas the early fruit sizing was not approached frequently. Concluding, the LiDAR based analysis provides an accurate tool for fruit counting.

When starting the LiDAR readings in the present study, foliage of deciduous trees was almost developed. The mean of LA_{LiDAR} increased slightly from 6.40 m^2 to 6.54 m^2 during the measuring period capturing the range between $DAFB_{65}$ and $DAFB_{130}$, respectively (Table 1). LA_{LiDAR} showed an overestimation at all measuring dates, presenting $MBE = 0.17 \text{ m}^2$ at $DAFB_{65}$ and 0.25 m^2 at last date. The manually measured leaf area was correlated to LA_{LiDAR} over the measuring period, showing an $R^2 = 0.89$ with $RMSE = 3.1 \%$ at $DAFB_{65}$ and $R^2 = 0.86$ with $RMSE = 6.4 \%$ at $DAFB_{130}$. The accuracy of the non-invasive analysis was limited due to occlusions and coinciding leaf surfaces as suggested in many plant species (Deery et al., 2021; Keller et al., 2022). However, such data derived from LiDAR point clouds are informative for crop load management, e.g. in late hand thinning of fruit considering the leaf area to fruit ratio (Penzel et al., 2021). According to the findings presented in Table 1, both information can be obtained with the same sensing technique.

7. Bivariate point density histogram at two wavelengths measured in laboratory and field conditions

The backscattered reflectance intensity measured with the two LiDAR sensors LiDAR₉₀₅ ($R_{ToF,905}$) and LiDAR₆₆₀ ($R_{ToF,660}$) were extracted from apple point clouds (Fig. 2) measured in laboratory conditions and in the orchard over the fruit growth period. Applying the

bivariate histogram of apple point clouds allowed to acquire the mean backscattered intensity (R_{ToF}) with the same point density from both laser scanners in dark room and in field measurements (Fig. 3). The number of points per apple increased with fruit size during the growth period, while the number of bin remained the same allowing a direct comparison between all fruit. R_{ToF} values found in previous work done on apple fruit, aimed at fruit segmentation, ranged between 60 % and 90 % measured at shortwave near infrared band of 905 nm (Gené-Mola et al., 2019). The same range was found in the present study for $R_{ToF,905}$ (Fig. 3). Comparing lab and field data, a sharper peak between 60 % and 80 % was found in field measurements. In field conditions, apple surface was captured by a lower number of points due to occlusions. The frequency distribution of $R_{ToF,905}$ hardly changed over the fruit growth period.

$R_{ToF,660}$ ranged from 0 to 80 % in the lab, whereas in field conditions the narrowed range between 0 and 40 % was captured. The $R_{ToF,660}$ showed lower values compared to $R_{ToF,905}$ due to chlorophyll absorption (Fig. 3). Furthermore, frequency curves were moving in direction from low to high intensity due to degradation of chlorophyll pigments, which corresponds to reduced absorption coefficient in riper fruit. The most frequent value in $R_{ToF,660}$ was found at 26.9 %, 33.8 %, 35.7 %, 41.3 %, and 63.6 % for $DAFB_{65}$, $DAFB_{75}$, $DAFB_{90}$, $DAFB_{105}$, and $DAFB_{130}$, respectively. However, in field conditions high overlap of $R_{ToF,660}$ intensity curves were found, with the most frequent value fluctuating with 18.1 %, 13.6 %, 23.5 %, 28.2 %, 27.9 % at $DAFB_{65}$, $DAFB_{75}$, $DAFB_{90}$, $DAFB_{105}$, $DAFB_{130}$, respectively.

From the merged point clouds the fruit $NDVI_{LiDAR}$ was calculated. The frequency curves of $NDVI_{LiDAR}$ showed a high variance and, during the growth period, moved in the direction from low to high intensity as can be assumed due to degradation of chlorophyll pigments which

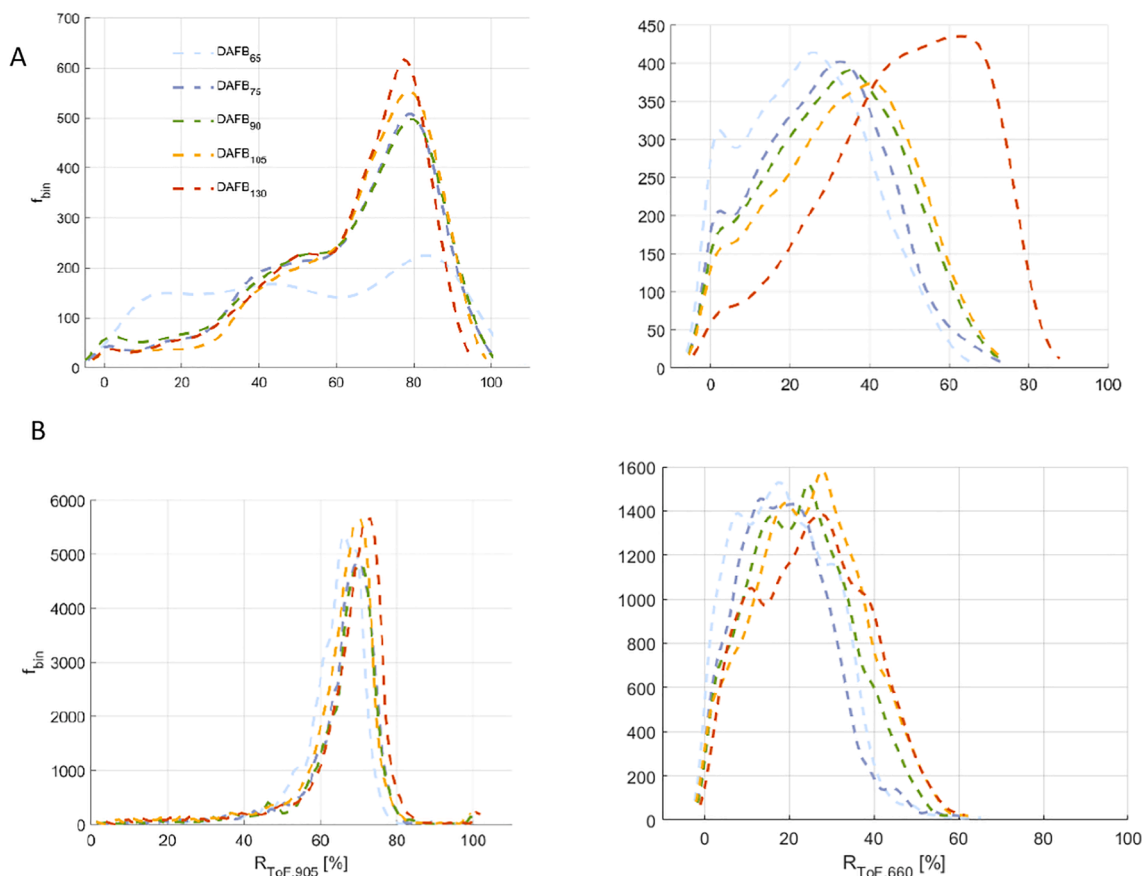


Fig. 3. Bivariate histogram considering all bins ($n = 160$ for each apple) of backscattered reflectance histogram (R_{ToF}) at five measuring dates during fruit development measured in A. laboratory ($n = 10$) and B. field ($n = 771$) for LiDAR₉₀₅ (left column) and LiDAR₆₆₀ (right column).

corresponds to the fruit ripening process (Fig. 4). More specifically, $NDVI_{LiDAR}$ ranged from 0.05 to 0.72 with a peak value of 0.34 at DAFB₆₅. The $NDVI_{LiDAR}$ values were reduced following chlorophyll degradation, reaching a peak value of 0.11 and a range between -0.25 and 0.38 at DAFB₁₃₀. Reduced ranges appeared in $NDVI_{LiDAR}$ measured in the orchard over the growing period (Fig. 4), again assumingly due to less points captured from the fruit in the partly overlapping foliage. Over the early measuring dates, the fruit $NDVI_{LiDAR}$ hardly changed. The last measuring date showed a clear decrease of $NDVI_{LiDAR}$ in the laboratory as well as in field measurements. Such findings, obtained non-invasively, are consistent with previous findings measured by means of spectroscopy with the sensor probe being in contact to the fruit surface (Zude-Sasse et al., 2002; Muresan et al., 2017).

8. Correlation of $NDVI_{LiDAR}$ and fruit reference analyses

For referencing purpose, after LiDAR scanning, the $NDVI_{Ref}$ was measured with a handheld spectrophotometer and the chlorophyll content (Chl_A , Chl_B , Chl_{pheo} and $Chl_{A+B+pheo}$) were chemical analysed over the growth period (Fig. 5). The temporal decrease of $NDVI_{Ref}$ was revealed, presenting a mean value of 0.88 ± 0.05 standard deviation at DAFB₆₅ and a mean value of -0.21 ± 1.21 at DAFB₁₃₀. The variability of Chl_A , Chl_B , Chl_{pheo} and its sum $Chl_{A+B+pheo}$ were enhanced at DAFB₆₅ and DAFB₇₅, and decreased during the following measuring dates. Single factor ANOVA revealed clear difference ($p < 0.001$) among all dates considering the spectral-optimally measured $NDVI_{Ref}$. Mean values of total chlorophyll content ($Chl_{A+B+pheo}$) were 0.98, 0.63, 0.46, 0.43 and 0.41 $mg\ cm^{-2}$ at DAFB₆₅, DAFB₇₅, DAFB₉₀, DAFB₁₀₅, and DAFB₁₃₀, respectively (Fig. 5).

The fruit $NDVI_{LiDAR}$ measured in dark room conditions of individual fruit ($n = 10$ at each measuring date) decreased from 0.36 at DAFB₆₅ to 0.13 at DAFB₁₃₀ (Table 2). A close relationship was observed between $NDVI_{Ref}$ and $NDVI_{LiDAR}$ at DAFB₁₃₀ ($R^2 = 0.85$, $RMSE = 2.12\%$), while low correlations were found at DAFB₆₅, DAFB₉₀, and DAFB₁₀₅. The Chl_A mean value ranged from 0.36 to $0.12 \cdot 10^{-2}\ mg/cm^2$ over the growth period. Generally, $NDVI_{LiDAR}$ showed enhanced correlation to Chl_A compared to other chlorophylls or the sum of chlorophylls over the growing period. More specifically, for Chl_A the R^2 of 0.85, 0.95, 0.82, 0.59, and 0.81 were found at DAFB₆₅, DAFB₇₅, DAFB₉₀, and DAFB₁₃₀, respectively. Concluding, the $NDVI_{LiDAR}$ was confirmed as an index for the chlorophyll content of fruit when measured in laboratory conditions. Earlier work on the NDVI of apple fruit measured by means of spectral-optical measurement in contact to the fruit report slightly enhanced correlations (Zude, 2003; Seifert et al., 2015). However, other vegetation indices captured with the available LiDAR sensors may be tested in future work (Zhang et al., 2021).

A linear model was used to express the overall relationship between

$NDVI_{Ref}$ and $NDVI_{LiDAR}$, revealing high $R^2 = 0.86$, $RMSE = 3.32\%$ calculated from the 3D point cloud of apples measured in the laboratory (Fig. 6). In parallel, the overall relationship between Chl_A and $NDVI_{LiDAR}$ was expressed with a logarithmic equation, revealing $R^2 = 0.81$, $RMSE = 3.98\%$ considering all measuring dates (Fig. 6).

In contrast to the laboratory measurements, mean values of $NDVI_{LiDAR}$ measured in the orchard showed higher range. The R^2 of mean fruit $NDVI_{LiDAR}$ and mean values of spectral-optimally measured fruit $NDVI_{Ref}$ was 0.65 considering all measuring dates (Table 3). However, low and moderate correlations were observed over fruit development with highest coefficients of determination at DAFB₇₅ ($R^2 = 0.51$, $RMSE = 1.58\%$) and DAFB₉₀ ($R^2 = 0.61$, $RMSE = 1.54\%$). Additionally, the mean fruit $NDVI_{LiDAR}$, measured in the orchard, was evaluated with the spectral-optimally measured mean $NDVI_{Ref}$ in low and high sections of the tree canopy (Fig. 7). The fruit measured in low section below 1.8 m, revealed $R^2 = 0.62$ (Fig. 7A), while $R^2 = 0.71$ was found in high sections > 1.8 m of canopy (Fig. 7B). The relationship of mean Chl_A and mean $NDVI_{LiDAR}$ separated at each measuring date appeared scattered. However, the overall range of mean Chl_A and mean $NDVI_{LiDAR}$ showed high relationship of $R^2 = 0.78$ and $RMSE = 1.31\%$. Furthermore, Chl_A measurements were separated in low and high sections of canopies, resulting in $R^2 = 0.41$ and $R^2 = 0.81$ at last measurement, respectively. The visually higher canopy density in lower tree section enhanced the error.

8.1. Impact of crop load on fruit $NDVI_{LiDAR}$

Destructive measurements of LA_{Ref} and points per tree (PPT) excluding points of wood were used to build a linear regression model for estimating the LA of each tree from the 3D tree point clouds (Fig. S1). Including all measuring dates, LA_{LiDAR} showed R^2 of 0.87 with $RMSE = 1.32\%$ and $R^2 = 0.96$ with 0.83%, in low and high sections of the tree, respectively. The mean of segmented leaf area by means of LA_{LiDAR} increased from 5.85 m^2 to 5.98 m^2 during measuring period in upper section (>1.8 m) of the tree, while lower tree section (<1.8 m) developed higher LA_{LiDAR} with 6.17 m^2 and 7.44 m^2 between DAFB₆₅ and DAFB₁₃₀, respectively.

The segmented LA_{LiDAR} and number of fruit ($Fruit_{LiDAR}$) were used to estimate the leaf area to fruit ratio ($LA_{LiDAR}:Fruit_{LiDAR}$) in low and high section of tree canopy (Fig. 8). The $LA_{LiDAR}:Fruit_{LiDAR}$ varied from 0.12 $m^2\ fruit^{-1}$ at DAFB₆₅ to 0.17 $m^2\ fruit^{-1}$ at DAFB₁₃₀ in low sections, while a higher range was found in the upper part of canopies reaching 0.31 $m^2\ fruit^{-1}$ at last measuring date. Clear difference was observed ($p < 0.001$) during fruit development in the two canopy sections. The highest percentage difference was found at last measuring date reaching 58.3%.

The fruit $NDVI_{LiDAR}$ showed no interaction with $LA_{LiDAR}:Fruit_{LiDAR}$

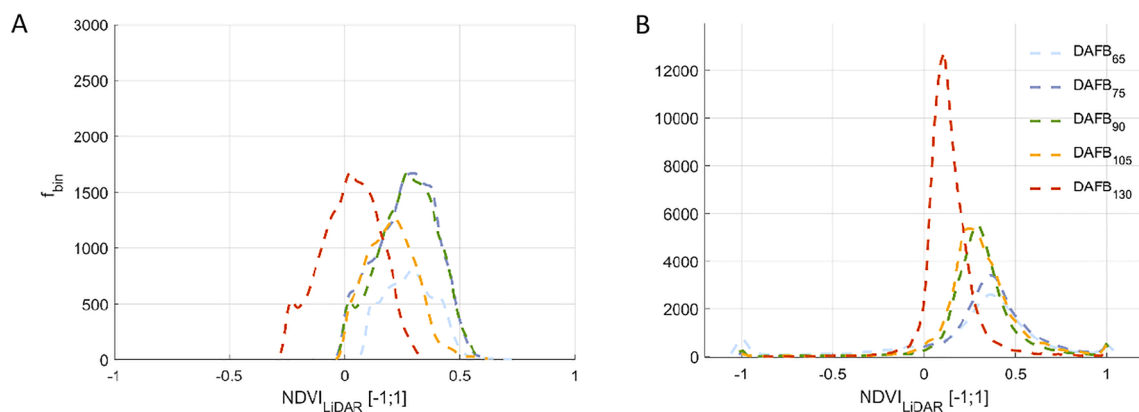


Fig. 4. Bivariate histogram of $NDVI_{LiDAR}$ considering all bins ($n = 160$ for each fruit) measured in A. dark room ($n = 10$) and B. orchard ($n = 771$) at five measuring dates during fruit development.

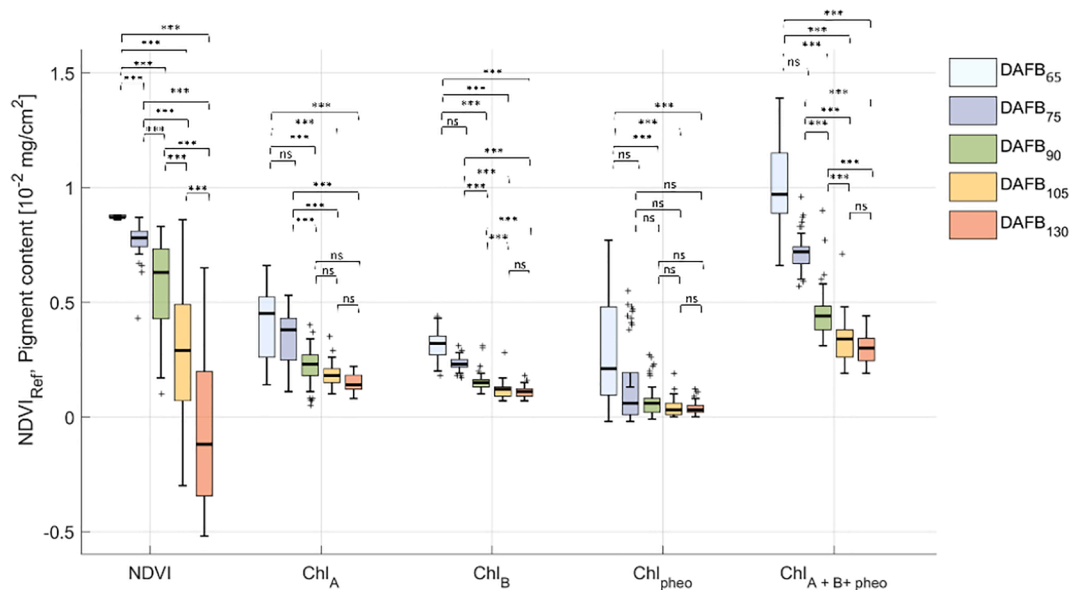


Fig. 5. $NDVI_{Ref}$ and fruit chlorophyll content during fruit development in day after full bloom (DAFB) ($n = 45$, total = 225). In each box, the centre line represents the mean value, the top and bottom of the box correspond to the 25th and 75th percentiles, and whiskers represent the 10th and 90th percentiles. Note: ‘***’ indicates a significant difference between groups ($p < 0.001$) and ‘ns’ indicates non-significant.

Table 2

Relationship of LiDAR derived fruit NDVI estimation ($NDVI_{LiDAR}$) measured in the laboratory ($n = 50$), fruit NDVI measured with handheld spectrophotometer ($NDVI_{Ref}$), and chemically analysed fruit chlorophyll content (Chl_A) in 10^{-2} mg/cm² at five measuring dates during apple growth provided in day after full bloom (DAFB).

		DAFB ₆₅	DAFB ₇₅	DAFB ₉₀	DAFB ₁₀₅	DAFB ₁₃₀
$NDVI_{LiDAR}$	Mean	0.36	0.35	0.29	0.26	0.13
	Max	0.47	0.42	0.34	0.33	0.29
	Min	0.28	0.24	0.24	0.17	0.07
$NDVI_{Ref}$	Mean	0.95	0.89	0.47	0.35	0.26
	RMSE (%)	5.15	2.12	3.43	4.54	2.12
	R^2	0.51	0.67	0.35	0.50	0.85
Chl_A	Mean	0.36	0.34	0.24	0.15	0.12
	RMSE (%)	3.13	5.25	3.22	5.05	3.63
	R^2	0.85	0.95	0.82	0.59	0.81

over the growth period. However, a logarithmic model was able to express the relationship of the two variables, considering the average values of each measuring date (Fig. 8). The $LA_{LiDAR}:Fruit_{LiDAR}$ correlated to fruit $NDVI_{LiDAR}$, revealing $R^2 = 0.71$ and $RMSE = 2.86\%$ in the upper canopy section, while similar $R^2 = 0.74$ with $RMSE = 2.46\%$ was observed in the lower section.

The manually measured fruit fresh mass showed the expected high correlation to manually measured fruit diameter (D_{Ref}) with R^2 of 0.95 and $RMSE$ of 0.86%. The fruit diameter derived by means of LiDAR scanning (D_{LiDAR}) showed a similar R^2 of 0.94 with $RMSE = 0.96\%$ (Figure S2). Using the LiDAR estimates of leaf area and fruit fresh mass allowed to monitor $LA_{LiDAR}:FM_{LiDAR}$ ratio during fruit growth. A steep decrease of $LA_{LiDAR}:FM_{LiDAR}$ was analysed between values at DAFB₆₅ and DAFB₇₅ in the entire canopy (Fig. 9A). Both curves, of low and high sections, showed a reciprocal trend that decreased due to fruit growth. At early measuring date, $LA_{LiDAR}:FM_{LiDAR}$ was reduced in the upper canopy section, revealing a mean value of 0.22 m²/g at DAFB₆₅. In the low section of canopy, 0.29 m²/g was found at DAFB₆₅. At the last

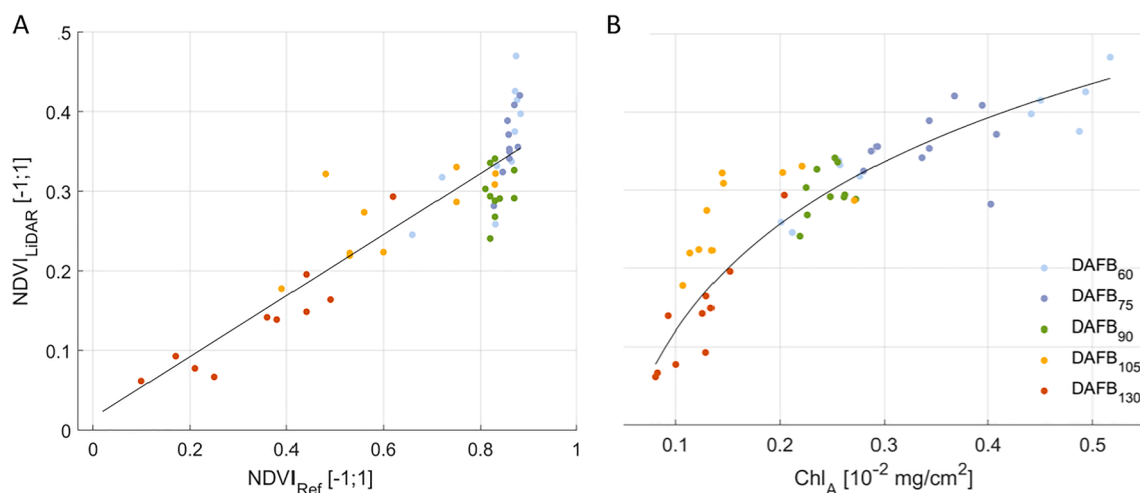


Fig. 6. Scatterplots of LiDAR derived fruit NDVI ($NDVI_{LiDAR}$) measured in the laboratory with A. manually measured $NDVI_{Ref}$ and B. chemically measured chlorophyll content at five measuring dates during fruit development of apples ($n = 50$).

Table 3

LiDAR derived mean fruit NDVI ($NDVI_{LiDAR}$) measured in the orchard with error analysis considering mean NDVI measured spectral-optimally in contact to the fruit at the tree ($NDVI_{Ref}$) ($n = 12$ trees) at five measuring dates during apple development provided in day after full bloom (DAFB).

		DAFB ₆₅	DAFB ₇₅	DAFB ₉₀	DAFB ₁₀₅	DAFB ₁₃₀	overall
$NDVI_{LiDAR}$	Mean	0.95	0.89	0.47	0.35	0.26	0.41
	RMSE (%)	1.54	1.58	1.54	2.87	2.26	0.58
	R^2	0.41	0.51	0.61	0.12	0.37	0.65

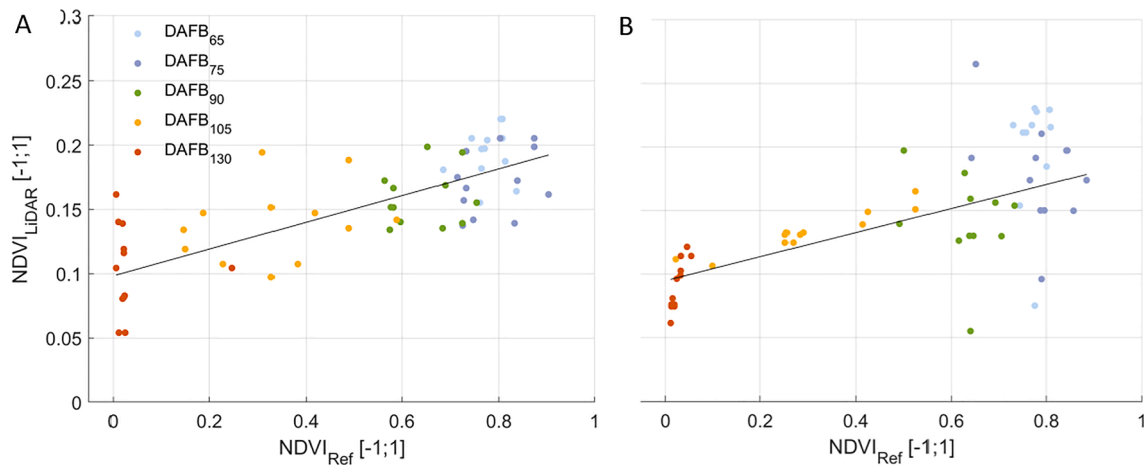


Fig. 7. Scatter plots of mean LiDAR derived NDVI ($NDVI_{LiDAR}$) and mean spectral-optimally measured $NDVI_{Ref}$ ($n = 12$) in A. low and B. high sections of the tree measured in the field, at five growth stages of apples provided in day after full bloom (DAFB).

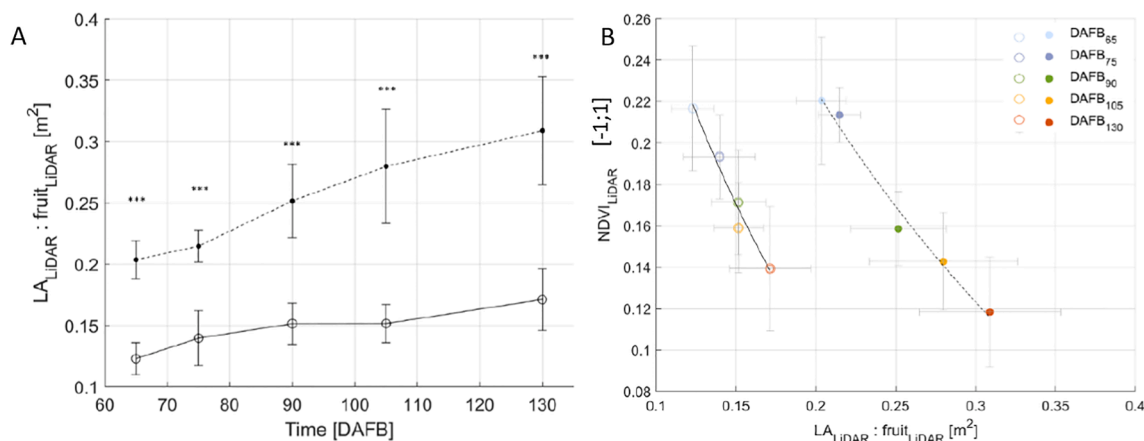


Fig. 8. A. Temporal development of leaf area to fruit ratio estimated by means of LiDAR (LA_{LiDAR} and $Fruit_{LiDAR}$) B. Regression analysis of $LA_{LiDAR}:Fruit_{LiDAR}$ ratio and fruit NDVI ($NDVI_{LiDAR}$) in low (open) and high (closed symbol) section of the canopy ($n = 12$) during fruit development in day after full bloom (DAFB). Note: “***” indicates a significant difference between classes ($p < 0.001$).

measuring date, DAFB₁₃₀, low and high sections of the canopy reached equal reduced value of $0.03 \text{ m}^2/\text{g}$ (Fig. 9).

In contrast to the $LA_{LiDAR}:Fruit_{LiDAR}$, moderate and high correlations were observed between $LA_{LiDAR}:FM_{LiDAR}$ and fruit $NDVI_{LiDAR}$ during fruit development. More specifically, R^2 of 0.43 and 0.71 was found at DAFB₆₅ and DAFB₁₃₀ in high canopy section, respectively. Lower parts of the tree revealed enhanced R^2 of 0.83 and 0.85, in earliest and last measurement, respectively.

Additionally to the analysis of fruit chlorophyll based on fruit $NDVI_{LiDAR}$, also the leaf $NDVI_{LiDAR}$ was measured. Earlier work showed high correlation of LiDAR data and leaf chlorophyll content (Hosoi et al., 2019; Sun et al., 2019). In the present work such, findings were confirmed for apple trees measured during fruit growth period, presenting moderate correlations (Figure S3). The leaf $NDVI_{LiDAR}$ was linearly related with the corresponding leaf Chl_A , resulting in $R^2 = 0.61$ and

$RMSE = 1.32 \%$ and $R^2 = 0.62$ with $RMSE = 1.12 \%$ in low and high section of canopies, respectively.

9. Conclusions

LiDAR 3D point clouds were acquired from apples in dark room and entire apple trees in field conditions. It was found that 660 and 905 nm wavelength of the LiDAR enabled to estimate the $NDVI_{LiDAR}$ point cloud of apples and leaves. The fruit $NDVI_{LiDAR}$ curves derived in the laboratory and field followed chlorophyll content degradation of apples during ripening. The fruit $NDVI_{LiDAR}$ resulted in high coefficient of determination with Chl_A ($R^2 = 0.81$) and $NDVI_{Ref}$ ($R^2 = 0.85$), when measured in dark room conditions. Less pronounced correlation of $NDVI_{LiDAR}$ to $NDVI_{Ref}$ were observed in the field, considering mean values of apples located in low ($R^2 = 0.62$) and high ($R^2 = 0.71$) sections of canopies.

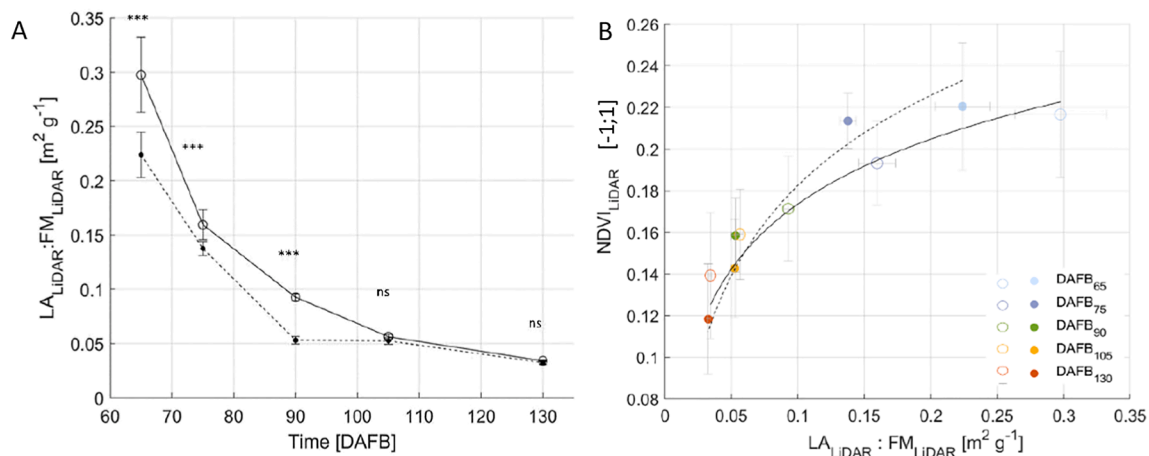


Fig. 9. A. Temporal development of leaf area to fruit fresh mass ratio measured by means of LiDAR ($LA_{LIDAR}:FM_{LIDAR}$), where “***” indicates significant difference between means ($p < 0.001$) and ‘ns’ indicates non-significant. B. Scatter plot of $LA_{LIDAR}:FM_{LIDAR}$ and fruit NDVI ($NDVI_{LIDAR}$) in low (open) and high (closed symbols) section of tree ($n = 12$) during fruit development in day after full bloom (DAFB).

The leaf area to fruit ratio derived by means of LiDAR interacted with the $NDVI_{LIDAR}$ of apples. Also, the regression curve of $LA_{LIDAR}:FM_{LIDAR}$ and $NDVI_{LIDAR}$ exhibited high correlations of $R^2 = 0.71$ and $R^2 = 0.85$ in high and low sections of the tree, respectively.

Overall, this study shows the applicability of LiDAR backscattered intensity to analyse the $NDVI_{LIDAR}$ and estimate the chlorophyll contents of fruit and leaves. LiDAR-derived data on crop load and chlorophyll content can support decision making of apple harvesting robots, find application in crop load management, and allow further physiological studies on fruit development.

Declaration of Competing Interest

The authors declare that they have no known competing financial interests or personal relationships that could have appeared to influence the work reported in this paper.

Data availability

Data will be made available on request.

Acknowledgements

We thank Gabi Wegner and Corinna Rolleczeck for manual rating and chemical lab analysis of fruit and acknowledge the technical support of Christian Regen in the setup of sensors on the conveyors and coding of data acquisition routine.

The project SPECTROFOOD is part of the ERA-NET Cofund ICT-AGRI-FOOD, with funding provided by national sources of BMEL and co-funding by the European Union’s Horizon 2020 research and innovation program, Grant Agreement number 2820ERA16H.

Appendix A. Supplementary data

Supplementary data to this article can be found online at <https://doi.org/10.1016/j.compag.2022.107611>.

References

Amplatzidis, Y., Partel, V., 2019. UAV-based high throughput phenotyping in citrus utilizing multispectral imaging and artificial intelligence. *Remote Sensing* 11 (4), 410. <https://doi.org/10.3390/rs11040410>.
 Anyamba, A., Tucker, C.J., 2005. Analysis of Sahelian vegetation dynamics using NOAA-AVHRR NDVI data from 1981–2003. *Journal of Arid Environments* 63 (3), 596–614. <https://doi.org/10.1016/j.jaridenv.2005.03.007>.

Ballester, C., Zarco-Tejada, P.J., Nicolás, E., Alarcón, J.J., Fereres, E., Intrigliolo, D.S., Gonzalez-Dugo, V.J.P.A., 2018. Evaluating the performance of xanthophyll, chlorophyll and structure-sensitive spectral indices to detect water stress in five fruit tree species. *Precision Agriculture* 19 (1), 178–193. <https://doi.org/10.1007/s11119-017-9512-y>.
 Bannari, A., Morin, D., Bonn, F., Huete, A.R., 1995. A review of vegetation indices. *Remote Sensing Reviews* 13, 95–120. <https://doi.org/10.1080/02757259509532298>.
 Biale, J.B., 1964. Growth, Maturation, and Senescence in Fruits: Recent knowledge on growth regulation and on biological oxidations has been applied to studies with fruits. *Science* 146 (3646), 880–888. <https://doi.org/10.1126/science.146.3646.880>.
 Cifuentes, R., Van der Zande, D., Salas-Eljatib, C., Farifteh, J., Coppin, P., 2018. A simulation study using terrestrial LiDAR point cloud data to quantify spectral variability of a broad-leaved Forest canopy. *Sensors* 18 (10), 3357. <https://doi.org/10.3390/s18103357>.
 Clawges, R., Vierling, L., Calhoun, M., Toomey, M., 2007. Use of a ground-based scanning lidar for estimation of biophysical properties of western larch (*Larix occidentalis*). *International Journal of Remote Sensing* 28 (19), 4331–4344. <https://doi.org/10.1080/01431160701243460>.
 Cusmano, Lucia, Miriam Koreen, and Lora Pissareva. 2018 OECD ministerial conference on SMEs: key issues paper. (2018).
 Dassot, M., Constant, T., Fournier, M., 2011. The use of terrestrial LiDAR technology in forest science: application fields, benefits and challenges. *Annals of Forest Science* 68, 959–974. <https://doi.org/10.1007/s13595-011-0102-2>.
 Deery, D.M., Smith, D.J., Davy, R., Jimenez-Berni, J.A., Rebetzke, G.J., James, R.A., 2021. Impact of varying light and dew on ground cover estimates from active NDVI, RGB, and LiDAR. *Plant Phenomics*, Article ID 9842178, 14 pages, 2021. <https://doi.org/10.34133/2021/9842178>.
 Delong, J.M., Harrison, P.A., Harkness, L., 2020. An optimal harvest maturity model for ‘Minneiska’ apple fruit based on the delta-absorbance meter. *The Journal of Horticultural Science and Biotechnology* 95, 637–644. <https://doi.org/10.1080/14620316.2020.1728199>.
 Eitel, J.U., Vierling, L.A., Long, D.S., 2010. Simultaneous measurements of plant structure and chlorophyll content in broadleaf saplings with a terrestrial laser scanner. *Remote Sensing of Environment* 114 (10), 2229–2237. <https://doi.org/10.1016/j.rse.2010.04.025>.
 FAO, 2022. FAO Global Statistical Yearbook, FAO Regional Statistical Yearbooks. <http://www.fao.org/faostat/en/#data/QL>, 12/23/2022.
 Gené-Mola, J., Gregorio, E., Guevara, J., Auat, F., Sanz-Cortiella, R., Escolà, A., Llorens, J., Morros, J.R., Ruiz-Hidalgo, J., Vilaplana, V., Rosell-Polo, J.R., 2019. Fruit detection in an apple orchard using a mobile terrestrial laser scanner. *Biosystems Engineering* 187, 171–184. <https://doi.org/10.1016/j.biosystemseng.2019.08.017>.
 Gongal, A., Karkee, M., Amatya, S., 2018. Apple fruit size estimation using a 3D machine vision system. *Information Processing in Agriculture* 5 (4), 498–503. <https://doi.org/10.1016/j.inpa.2018.06.002>.
 Han, Z., Hu, Y., Lv, Y., Rose, J.K., Sun, Y., Shen, F., Wang, Y., Zhang, X., Xu, X., Wu, T., Han, Z., 2018. Natural variation underlies differences in ETHYLENE RESPONSE FACTOR17 activity in fruit peel degreening. *Plant Physiol* 176 (3), 2292–2304.
 Hewitt, S., Dhingra, A., 2020. Beyond ethylene: new insights regarding the role of alternative oxidase in the respiratory climacteric. *Frontiers in Plant Science* 11, 1578. <https://doi.org/10.3389/fpls.2020.543958>.
 Hosoi, F., Umeyama, S., Kuo, K., 2019. Estimating 3D chlorophyll content distribution of trees using an image fusion method between 2D camera and 3D portable scanning lidar. *Remote Sensing* 11 (18), 2134. <https://doi.org/10.3390/rs11182134>.
 Jones, J.D., Hulme, A.C., Wooltorton, L.S.C., 1965. The respiration climacteric in apple fruits: Biochemical changes occurring during the development of the climacteric fruit

- detached from the tree. *New Phytologist* 64 (1), 158–167. <https://doi.org/10.1111/j.1469-8137.1965.tb05383.x>.
- Kasimati, A., Espejo-García, B., Darra, N., Fountas, S., 2022. Predicting grape sugar content under quality attributes using normalized difference vegetation index data and automated machine learning. *Sensors* 22 (9), 3249. <https://doi.org/10.3390/s22093249>.
- Keller, B., Zimmermann, L., Rascher, U., Matsubara, S., Steier, A., Müller, O., 2022. Toward predicting photosynthetic efficiency and biomass gain in crop genotypes over a field season. *Plant Physiology* 188, 301–317. <https://doi.org/10.1093/plphys/kiab483>.
- Knee, M., 1980. Methods of measuring green colour and chlorophyll content of apple fruit. *Journal of Food Technology* 15, 493–500.
- Kuckenbergh, J., Tartachnyk, I., Noga, G., 2008. Evaluation of fluorescence and remission techniques for monitoring changes in peel chlorophyll and internal fruit characteristics in sunlit and shaded sides of apple fruit during shelf-life. *Postharvest Biology and Technology* 48, 231–241. <https://doi.org/10.1016/j.postharvbio.2007.10.013>.
- Li, Y., He, N., Hou, J., Xu, L., Liu, C., Zhang, J., Wang, Q., Zhang, X., Wu, X., 2018. Factors influencing leaf chlorophyll content in natural forests at the biome scale. *Frontiers in Ecology and Evolution* 6, 64. <https://doi.org/10.3389/fevo.2018.00064>.
- Merzlyak, M.N., Gitelson, A.A., Chivkunova, O.B., Raktin, V.Y., 1999. Non-destructive optical detection of pigment changes during leaf senescence and fruit ripening. *Physiologia plantarum* 106 (1), 135–141. <https://doi.org/10.1034/j.1399-3054.1999.106119.x>.
- Muresan, E.A., Muste, S., Muresan, C.C., Mudura, E., Paucean, A., Stan, L., Vlaic, R.A., Cerbu, C.G., Muresan, V., 2017. Assessment of Polyphenols, Chlorophylls, and Carotenoids during Developmental Phases of Three Apple Varieties. *Romanian Biotechnological Letters* 22, 12546–12553.
- Nelson, R.C., 1940. Quantitative study of the production of ethylene by ripening McIntosh apples. *Plant Physiology* 15 (1), 149. <https://doi.org/10.1104/pp.15.1.149>.
- Peña, M.A., Liao, R., Brenning, A., 2017. Using spectrotemporal indices to improve the fruit-tree crop classification accuracy. *ISPRS Journal of Photogrammetry and Remote Sensing* 128, 158–169. <https://doi.org/10.1016/j.isprsjprs.2017.03.019>.
- Penzel, M., Herppich, W.B., Weltzien, C., Tsoulias, N., Zude-Sasse, M., 2021. Modeling of Individual Fruit-Bearing Capacity of Trees Is Aimed at Optimizing Fruit Quality of *Malus x domestica* Borkh. 'Gala'. *Front Plant Sci* 1323.
- Pflanz, M., Zude, M., 2008. Spectrophotometric analyses of chlorophyll and single carotenoids during fruit development of tomato (*Solanum lycopersicum* L.) by means of iterative multiple linear regression analysis. *Applied Optics* 47 (32), 5961–5970.
- Rouse Jr, J.W., Haas, R.H., Schell, J.A. and Deering, D.W., 1973. *Monitoring the vernal advancement and retrogradation (green wave effect) of natural vegetation* (No. NASA-CR-132982).
- Seifert, B., Zude, M., Spinelli, L., Torricelli, A., 2015. Optical properties of developing pip and stone fruit reveal underlying structural changes. *Physiologia Plantarum* 153 (2), 327–336. <https://doi.org/10.1111/ppl.12232>.
- Seifert, B., Zude-Sasse, M., 2016. High hydrostatic pressure effects on spectral-optical variables of the chlorophyll pool in climacteric fruit. *LWT* 73, 303–310. <https://doi.org/10.1016/j.lwt.2016.06.011>.
- Solovchenko, A.E., Chivkunova, O.B., Merzlyak, M.N., Gudkovsky, V.A., 2005. Relationships between chlorophyll and carotenoid pigments during on-and off-tree ripening of apple fruit as revealed non-destructively with reflectance spectroscopy. *Postharvest Biology and Technology* 38, 9–17. <https://doi.org/10.1016/j.postharvbio.2005.05.004>.
- Sun, J., Shi, S., Yang, J., Gong, W., Qiu, F., Wang, L., Chen, B., 2019. Wavelength selection of the multispectral lidar system for estimating leaf chlorophyll and water contents through the PROSPECT model. *Agricultural and Forest Meteorology* 266, 43–52. <https://doi.org/10.1016/j.agrformet.2018.11.035>.
- Tsoulias, N., Paraforos, D.S., Fountas, S., Zude-Sasse, M., 2019. Estimating canopy parameters based on the stem position in apple trees using a 2D lidar. *Agronomy* 9 (11), 740. <https://doi.org/10.3390/agronomy9110740>.
- Tsoulias, N., Paraforos, D.S., Xanthopoulos, G., Zude-Sasse, M., 2020. Apple shape detection based on geometric and radiometric features using a LiDAR laser scanner. *Remote Sensing* 12 (15), 2481. <https://doi.org/10.3390/rs12152481>.
- Tsoulias, N., Xanthopoulos, G., Fountas, S., Zude-Sasse, M., 2022. Effects of soil ECa and LiDAR-derived leaf area on yield and fruit quality in apple production. *Biosystems Engineering* 223, 182–199. <https://doi.org/10.1016/j.biosystemseng.2022.03.007>.
- Tucker, C.J., Pinzon, J.E., Brown, M.E., Slayback, D.A., Pak, E.W., Mahoney, R., Vermote, E.F., El Saleous, N., 2005. An extended AVHRR 8-km NDVI dataset compatible with MODIS and SPOT vegetation NDVI data. *International journal of remote sensing* 26 (20), 4485–4498. <https://doi.org/10.1080/01431160500168686>.
- Underwood, J.P., Hung, C., Whelan, B., Sukkarieh, S., 2016. Mapping almond orchard canopy volume, flowers, fruit and yield using lidar and vision sensors. *Computers and Electronics in Agriculture* 130, 83–96. <https://doi.org/10.1016/j.compag.2016.09.014>.
- Walsh, K.B., Blasco, J., Zude-Sasse, M., Sun, X., 2020. Visible-NIR 'point' spectroscopy in postharvest fruit and vegetable assessment: The science behind three decades of commercial use. *Postharvest Biology and Technology* 168, 111246. <https://doi.org/10.1016/j.postharvbio.2020.111246>.
- Watt, P.J., Donoghue, D.N.M., 2005. Measuring forest structure with terrestrial laser scanning. *International Journal of Remote Sensing* 26 (7), 1437–1446. <https://doi.org/10.1080/01431160512331337961>.
- Wei, G., Song, S., Zhu, B., Shi, S., Li, F., Cheng, X.W., 2012. Multi-wavelength canopy LiDAR for remote sensing of vegetation: Design and system performance. *ISPRS Journal of Photogrammetry and Remote Sensing* 69, 1–9. <https://doi.org/10.1016/j.isprsjprs.2012.02.001>.
- Zhang, J., Tian, H., Wang, D., et al., 2021. A novel spectral index for estimation of relative chlorophyll content of sugar beet. *Computers and Electronics in Agriculture* 184, 106088.
- Zhou, L., Tucker, C.J., Kaufmann, R.K., Slayback, D., Shabanov, N.V., Myneni, R.B., 2001. Variations in northern vegetation activity inferred from satellite data of vegetation index during 1981 to 1999. *Journal of Geophysical Research: Atmospheres* 106 (D17), 20069–20083. <https://doi.org/10.1172/JCI13505>.
- Ziosi, V., Noferini, M., Fiori, G., Tadiello, A., Trainotti, L., Casadoro, G., Costa, G., 2008. A new index based on vis spectroscopy to characterize the progression of ripening in peach fruit. *Postharvest Biology and Technology* 49, 319–329.
- Zude, M., 2003. Comparison of indices and multivariate models to non-destructively predict the fruit chlorophyll by means of visible spectrometry in apple fruit. *Analytica Chimica Acta* 481 (1), 119–126. [https://doi.org/10.1016/S0003-2670\(03\)00070-9](https://doi.org/10.1016/S0003-2670(03)00070-9).
- Zude-Sasse, M., Truppel, I., Herold, B., 2002. An approach to non-destructive apple chlorophyll determination. *Postharvest Biology and Technology* 25, 123–133. [https://doi.org/10.1016/S0925-5214\(01\)00173-9](https://doi.org/10.1016/S0925-5214(01)00173-9).
- Zude-Sasse, M., Fountas, S., Gemtos, T.A., Abu-Khalaf, N., 2016. Applications of precision agriculture in horticultural crops – review. *European Journal of Horticultural Science* 81, 78–90. <https://doi.org/10.17660/eJHS.2016/81.2.2>.